Formation of Surface Defects Dominates Ion Migration in Lead-Halide Perovskites

Daniele Meggiolaro,[a,b] Edoardo Mosconi,[a]* Filippo De Angelis [a,b,c] *

[a] *Computational Laboratory for Hybrid/Organic Photovoltaics (CLHYO), Istituto CNR di Scienze e Tecnologie Molecolari (ISTM-CNR), Via Elce di Sotto 8, 06123, Perugia, Italy.*

[b]*CompuNet, Istituto Italiano di Tecnologia, Via Morego 30, 16163 Genova, Italy.*

[c] *Department of Chemistry, Biology and Biotechnology, University of Perugia, Via Elce di Sotto 8, 06123, Perugia, Italy.*

E-mail: filippo@thch.unipg.it

Abstract

We propose a new model of defect formation and ion migration at the surfaces / grain boundaries of lead-halide perovskites, based on *ab initio* calculations. Inspired by the spread of experimentally measured activation energies for ion migration in similar lead-iodide perovskites, we define an effective defect formation energy weighed upon surface and bulk contributions. We thus link the large variation in measured activation energies for ion migration to the different defect formation energy of polycrystalline thin films with different grains size. Defect formation is facilitated at surfaces, thus smaller grains exhibit an averagely lower activation energy to ion migration than larger grains. We also account for the increased ion migration observed under light. On overall, our findings point at surface passivation as a major issue to stabilize lead-halide perovskites against formation of defects, limiting in turn the decomposition reactions associated to defect photochemistry.

TOC Graphics
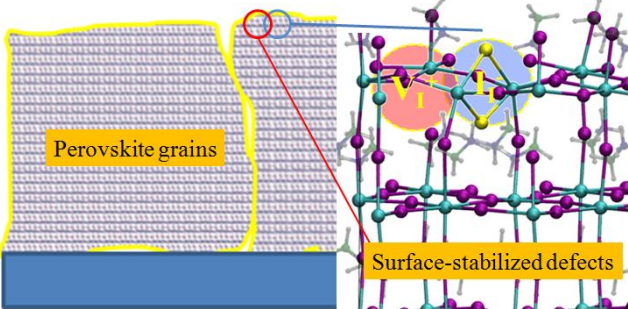
The success of metal-halide perovskites (MHPs) in optoelectronic devices has revolutionized the landscape of applications dominated by traditional semiconductors. The outstanding absorption, charge generation and transport properties of MHPs[1, 2] apparently contrasts with the paradigm of high-purity/high quality semiconductors made under controlled conditions. MHPs achieve similar performance in devices than the former but, by contrast, are fabricated by solution-processing techniques at low temperature from medium-purity precursor compounds.

The relatively weak metal-halide bond of MHPs (formation enthalpies <0.2 eV per formula unit) [3] gives rise to an inherently soft crystal lattice which is prone to dynamical and structural disorder, associated to formation of defects.[4] Defects introducing levels in the material's band-gap may act as traps and recombination centers for photogenerated charge carriers, limiting the device performance and impacting the device temporal stability. The moderately high trap density typical of solution-made polycrystalline thin films used in solar cells (10^{15}-10^{16} defects per cm^3) was found to marginally affect the efficiency of the ensuing devices.[5] The reasons lying behind defect tolerance in MHPs are still actively researched [6,7] to possibly export the same tolerance in a diverse set of semiconductors.[8] Among native point defects those related to excess halides (*i.e.* interstitial iodine) or analogously undercoordinated halides - *e.g.* metal vacancies - can represent a significant trap source in lead-halide perovskites.[6, 9] Halide vacancies act as shallow traps but they may play a major role in affecting the material stability.[10] In the prototypical MAPbI$_3$ perovskite (MA=methylammonium) MA interstitials are also fairly abundant at the native (close to intrinsic) Fermi level but such defects do not introduce electronic states in the gap.[11] Defect complexes, such as Schottky or Frenkel defects, may alter the defect density predicted for point defects by introducing compensating equilibria among different vacancies or among vacancies and interstitials,[14, 31] respectively.

Defects may also introduce ionic mobility channels in MHPs.[12] The migration of halides is boosted by the presence of vacancy and interstitial defects, acting as shuttles for halide hopping.[13, 14]

There clearly exists a strict connection between the energetics of defect formation and the entity of ion migration. If the migrating defects are also charge traps, as it occurs for iodine defects,[15] the migrating defects can respond to the action of an electric field and to the presence of photo-generated carriers.[16] Further complicating the scenario, some of the defect traps may undergo photochemical reactions, whose most evident manifestation is the release of molecular iodine under light irradiation.[17, 18]

Ion migration in MHPs has been investigated in depth, both experimentally and theoretically, disclosing the nature of migrating ions and the associated time scales. Considerable knowledge on this phenomenon has built up in the literature, pointing at halides as the most mobile species.[19-22] A large variation in the measured activation energies for ion migration in MHPs has been reported, with experimental values spanning about one order of magnitude, ranging from ~0.1 to ~1.0 eV.[14, 15, 19-24] Calculated values also showed a significant variation, ranging from ~0.1 to ~0.6 eV, but they consistently showed the same order of activation energies, with halide defects faster (or at most equally fast) than A-cations, which are in turn faster than Pb defects.[13, 14, 19, 20, 25-28] While variations in calculated activation energies, albeit unexpected, can be traced back to the different simulation size and structural models (*e.g.* cubic *vs.* tetragonal) and details of the computations (level of theory, method to calculate the transition states, orientation of the A-cations etc.), the variation in measured activation energies for ion migration deserves further attention. This large spread in experimental and calculated values has basically made it impossible to unambiguously assess the nature of the migrating ions based on comparison of the two data sets. Adding to this puzzling picture, a significant light-induced enhancement of ion migration has been reported, whose origin is still debated.[18, 29] A possibly related phenomenon is the notorious phase de-mixing of mixed-halide perovskites under light,[30] which limits the photostability of technologically relevant intermediate compositions for tandem devices. Since ion migration must be

involved in halide de-mixing, a role of defects (and possibly charge traps) emerges also in such unusual behavior.[31, 32]

An important observation which may help in rationalizing the spread of experimental values is the variation of measured activation energies with the grain size of polycrystalline thin films samples and single crystals. Xing *et al.* reported temperature dependent conductivity measurements showing that the measured activation energies obtained by Arrhenius fitting of conductivity data in the dark (and under light exposure) significantly increased with grain size.[29] The activation energies measured in the dark increased from ~0.3 eV for ~300 nm to ~0.5 eV for ~1μm sized-grains, up to ~1.0 eV for mm-scale single crystals, indicative of an increasingly difficult ion migration in large grains or crystals. This activation energy variation with grain size is intriguing and may reveal important features about the nature of ion migration.

Starting from basic conductivity equations and combining experimental observations with high level *ab initio* calculations, we develop a new model of surface-assisted defect formation and apply it to ion migration in MAPbI$_3$. Our model accounts for the variation of ion migration activation energy with grain size and light, revealing a fundamental role of surface defects in affecting ion migration.

To clarify the factors potentially affecting the measured activation energies it is useful to illustrate the basic equations ruling conductivity. The conductivity (σ) is defined as:

$$\sigma = nZe\mu \tag{1}$$

where n is the is the volume density of charge carriers, Z is their charge, e is the electron charge and μ is the carriers mobility, which is a measure of the drift velocity in a constant electric field. Using the Nernst-Einstein relation the ionic conductivity can be expressed in terms of the diffusion coefficient of the migrating ion, D:

$$\sigma = ne^2 D/kT \tag{2}$$

where k is the Boltzmann constant and T the absolute temperature.

The diffusion coefficient has an exponential dependence on the temperature:

$$D=(\nu_0 \, d^2/6) \, exp(\Delta S^{\neq}/k) \, exp(-\Delta H^{\neq}/kT) \tag{3}$$

where ν_0 is the attempt frequency of an ionic jump, d is jump distance, $\Delta S^{\neq}$ is the entropy variation related to the ionic jump and $\Delta H^{\neq}$ is the microscopic energy barrier. ν_0, typically the vibrational frequency of the bond being broken or loosened during the jump, $\sim 10^{12}$ Hz, is weakly temperature dependent, with a form of the type $1/T^m$, with $m=1,0$ or ½.

$\Delta H^{\neq}$ is the energy barrier to migration, *i.e.* the energy it takes for an ion to reach the transition state connecting the starting and final equilibrium structures, see examples in Figure 1, and it is the quantity calculated by *ab initio* calculations (typically not including thermal/vibrational corrections), see Table 1.

Equation (3) can be re-written as:

$$D=D^0/T^m \, exp(-\Delta H^{\neq}/kT) \tag{4}$$

where D_0 is a constant for a given defect/material combination.

We can notice that eq. (1) and (2) both contain n, which in absence of extrinsic doping corresponds to the density of mobile defects. As such n is related to the free energy of defect formation, *i.e.* the defect formation energy (*DFE*) by:

$$n=N \, exp \, (-DFE/kT) \tag{5}$$

where N is the density of available defect sites (in cm^{-3}). In some derivations[33] the DFE is divided by a factor 2 to account for the formation of defect pairs (*i.e.* Schottky or Frenkel defects).

Equation (2) can thus be re-written as:

$$\sigma = T^m \, e^2 D_0/kT \, exp(-\Delta H^{\neq}/kT) \, exp \, (-DFE/kT) \tag{6}$$

When $m=0$, plotting $ln(\sigma T)$ vs. $1/T$ provides a straight line from which the activation energy (E_a) can be extracted. The T^m temperature dependence is sufficiently weak compared to the exponential term that even if $m=1$ or ½ a linear trend is still usually retrieved.[33]

We can now express eq. (6) as:

$\sigma = \sigma_0/kT \; exp(-Ea/kT)$ (7)

with $\sigma_0 = T^m e^2 D_0$ and

$E_a = \Delta H^{\neq} + DFE$ (8)

For a system in thermodynamic equilibrium and in the absence of extrinsic defects, the activation energy measured in conductivity experiments, E_a in eq. 7, contains two terms: *i)* the migration energy barrier, $\Delta H^{\neq}$; and *ii)* the defect formation energy, *DFE*, as per eq. (8). Thus by plotting *ln(σT)* vs. *1/T* the slope of the linear data fit is $E_a = \Delta H^{\neq} + DFE$. *This means that one cannot disentangle*, at least in principle, *the energy barrier for an ionic jump ($\Delta H^{\neq}$) from the energy required to form the defect undergoing the jump (DFE)*, as they both show an exponential dependence on temperature.

The E_a variation with grain size[29] can now be interpreted as a variation in the individual $\Delta H^{\neq}$ and *DFE* terms, or a combination of the two. Since $\Delta H^{\neq}$ is a microscopic quantity related to the intimate properties of the involved chemical bonds, this is likely less affected by the grain size or by the different properties of surfaces *vs.* bulk. As an example, we calculate a comparable migration energy barrier (~0.1 eV at the PBE level, see Supporting Information for details) for negative interstitial iodine in bulk MAPbI$_3$ and at the (001) MAI-terminated and PbI$_2$-terminated surface, see Figure 1 and Supporting Information. This is consistent with calculations by Oranskaia *et al.* [28] on MA- and FAPbBr$_3$ showing a variation of migration energy barrier for halide vacancies and interstitials within 0.1-0.2 eV in bulk and surfaces. We notice, however, that some uncertainty exists on the nature of surfaces in lead-halide perovskites, due to the surface restructuring and disordering experimentally observed which may induce additional variability.[34, 35]
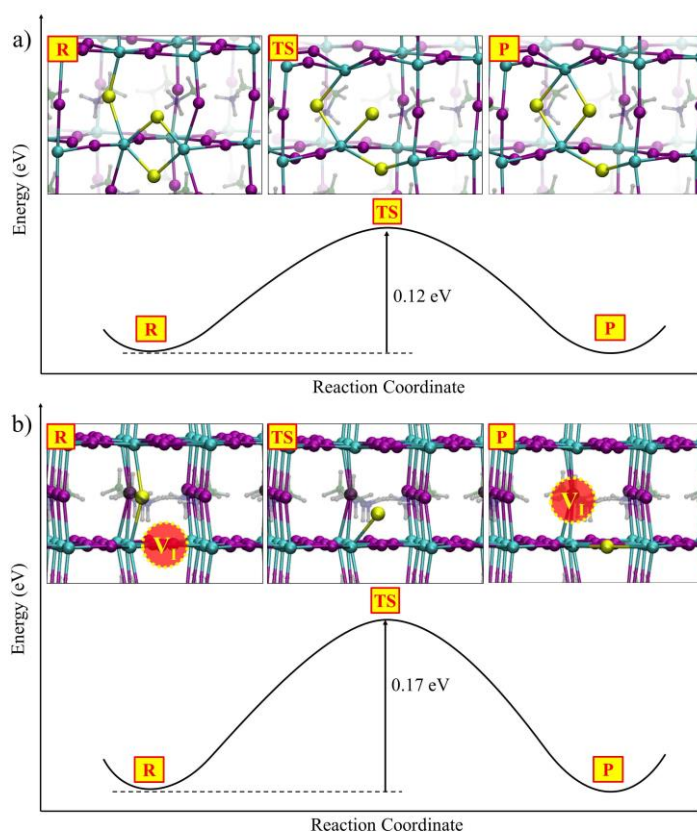
Figure 1. Reaction energy profile for the migration process of the interstitial (a) and iodide vacancy (b) in the MAPbI$_3$ bulk. The reagent (R), transition state (TS) and product (P) structures are also shown. R and P are shown at the same energy in both cases. The calculated migration energy barrier for the two processes is reported.

Since $\Delta H^{\neq}$ does not show significant variations between bulk and surfaces, the measured E_a change with grain size is likely led by the different *DFE*. *We propose variation in this term to be associated to the availability of surface sites to host defects*. We focus in particular on iodine Frenkel defects (I_i^-/ V_I^+ - I_i^-=negative interstitial iodine, V_I^+=positive iodine vacancy), which have been recently proposed to be formed and to migrate under the influence of an electric field in MAPbI$_3$,[36, 37] but analogous considerations may likely hold for Schottky defects.[31] Notice that the indicated defect charges are those formally expected from a negative iodine and the related vacancy but the actual charge bore by the defect may differ due to covalency and delocalization effects. Forming an interstitial iodine at the surface is likely favored compared to the bulk, since the steric hindrance

8

required to accommodate the extra iodine in the lattice is relieved on the surface, and undercoordinated Pb atoms may favorably bind the interstitial atom. As a matter of fact, strong stabilization of interstitial iodine defects was found on MAPbI$_3$ surfaces exposing undercoordinated Pb atoms compared to the bulk.[6, 38] A similar surface stabilization is calculated here for a I$_i^-$/V$_I^+$ Frenkel pair, whose formation becomes increasingly favored by considering surfaces with an increasing fraction of undercoordinated surface Pb atoms, up to the point of becoming spontaneous on PbI$_2$-terminated surfaces, see Figure 2.
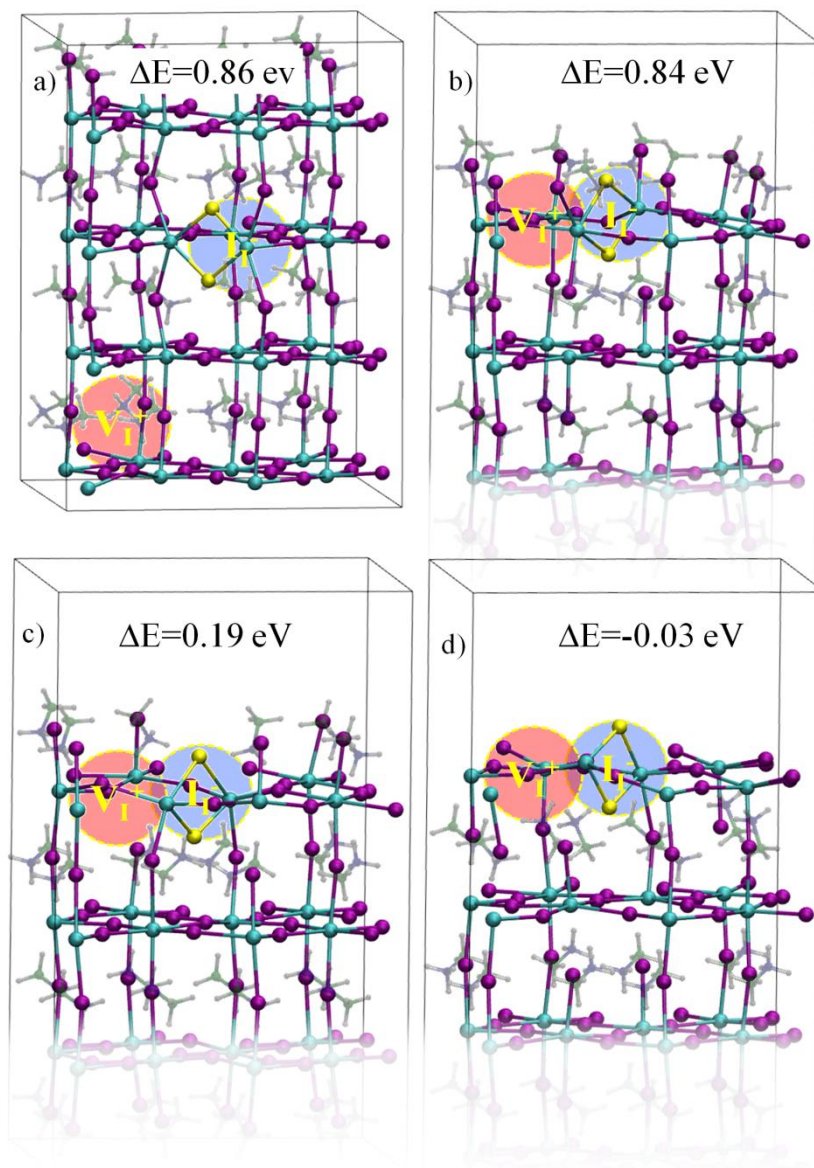
Figure 2. Optimized structures and formation energies (eV) for I$_i^-$/ V$_I^+$ Frenkel pair in MAPbI$_3$ bulk (a); and at MAI-terminated (b), MAI-vacant (c) and PbI$_2$-terminated surfaces, corresponding to an

increasing fraction of undercoordinated surface Pb atoms. Defect formation energies calculated at the PBE level are also reported (eV). Notice that these values differ from those of Table 1 which are more accurately calculated by HSE-SOC.

Table 1. DFE of I_i^-, I_i^0, V_I^+, V_I^0 and non interacting I_i^-/ V_I^+ Frenkel pair (sum of the individual defects) under iodine medium conditions in bulk MAPbI$_3$ calculated by HSE-SOC including dispersion corrections through Grimme's D3 approach[39] on a 2x2x2 supercell with structures optimized by PBE. Migration energy barriers ($\Delta H^{\neq}$) for I_i^-, I_i^0, V_I^+, V_I^0 are also reported, as calculated by HSE-SOC structural relaxation in a bulk 2x2x1 supercell. Values in parenthesis are calculated by PBE on the same bulk 2x2x1 supercell.

Defect	DFE	$\Delta H^{\neq}$
I_i^-	0.55	0.12 (0.10)
I_i^0	1.03	0.18
V_I^+	0.81	0.17 (0.12)
V_I^0	1.70	0.17
I_i^- / V_I^+	1.36	-

The proposed surface-stabilized defect formation is consistent with the effect of surface passivating species in stabilizing solar cell devices[40] and in dimming mixed halide perovskite de-mixing[41] and it can be interpreted as a reduction of surface sites available for defect formation. It also provides an explanation for the effect of surface chlorine and Lewis bases leading to grains with higher photoluminescence quantum yield and to improved photovoltaic performance in polycrystalline MAPbI$_3$ films.[42-44]

Notably, a similar migration energy barrier is calculated for I_i^- and V_I^+ indicative of balanced migration energy barriers for iodine Frenkel defects.[36, 37] Also technically notable, the computationally expensive and in principle more accurate HSE-SOC structural relaxations delivering the $\Delta H^{\neq}$ values of Figure 1 and Table , provide comparable energy barriers for charged

iodine defects to those previously obtained by the less computationally demanding PBE calculations (~0.1 eV).[13]

Based on these combined results, *we propose that the varying E_a measured for different crystal/grain size is related to the accessibility of surface sites which stabilize defect formation, leading to a DFE reduction*. We thus rewrite the average DFE affecting the defect density through eq. (5) as the sum of surface and bulk contributions, weighed by their respective density:

$$DFE_{av} = (f_{surf} DFE_{surf} + f_{bulk} DFE_{bulk})/(f_{surf} + f_{bulk}) \tag{9}$$

where f_{surf} (f_{bulk}) and DFE_{surf} (DFE_{bulk}) are the number density and formation energies of defects at the surface (bulk). Eq. (9) describes an average *DFE* that is weighed upon the occupation of surface and bulk defect sites. We can elaborate further on this model considering the variation in surface/volume ratio of crystalline grains. If we take for simplicity cubic grains, the total available surface (including grain boundaries) scales as $\sim 6L^2$, while the volume scales as $\sim L^3$, where L is the grain dimension, see Scheme 1.
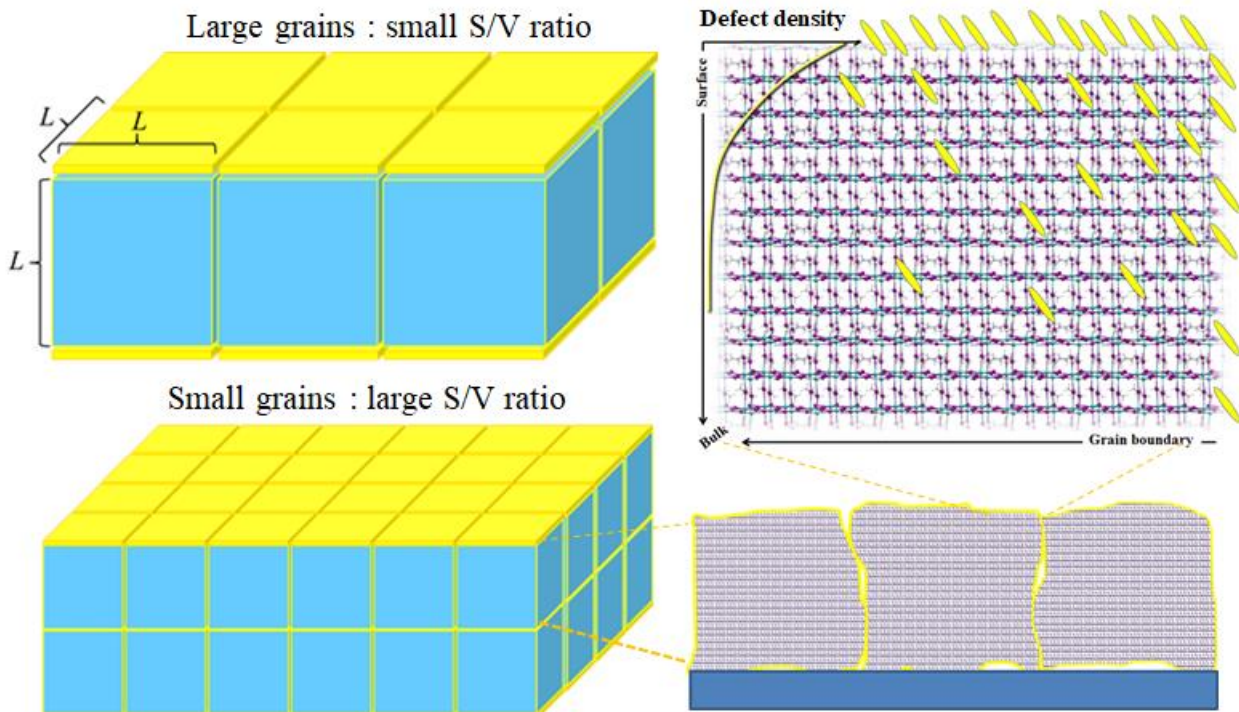
Scheme 1. Schematic illustration of surface/volume ratio in polycrystalline thin films. Large grains (L=cubic grain size) and small grains differ in their surface/volume (S/V) ratio. Also shown is a schematic representation of a thin film with zoom on the grain boundary and surface showing the

corresponding different defect distributions (yellow ellipses). Notice the drastic reduction of defects going from the surface/grain boundaries to the bulk.

The *DFE* of eq. (9) averaged over surface and bulk defects can thus be approximately expressed as:

$$DFE_{av}=(d_{surf}6L^2 DFE_{surf} + d_{bulk}L^3 DFE_{bulk})/(d_{surf} 6L^2 + d_{bulk}L^3)$$

(10)

where we have taken $f_{surf} = d_{surf}6L^2$ and $f_{bulk}=d_{bulk}L^3$, with d_{surf} and d_{bulk} the density of sites on which a defect can be formed on the surface and bulk, respectively.

To estimate the DFE_{surf} and DFE_{bulk} terms we refer to experimental values by Xing *et al.* [29] We know that for ~300 nm grain size the measured activation energy in the dark is ~0.3 eV. We know that this is the sum of $\Delta H^{\neq}$ (calculated value ~0.1 eV) and the site-averaged DFE_{av}, of eq. (9) and (10). By difference we thus calculate $DFE_{av} = 0.2$ eV for L=300 nm, which allows us to fix the DFE at low L values. Similarly, knowing that E_a is ~1 eV for single crystals we take $DFE_{av} = 0.9$ eV for large L, so we can univocally define the function $DFE_{av}(L)$, shown in Figure 3. We may further elaborate on whether the accessible surface is $6L^2$ or a lower fraction (*e.g.* $2L^2$), accounting for the partial passivation of surface sites at grain boundaries or at the substrate interface, but the results are only moderately affected by this choice, as illustrated below. We can now test our model and check whether it reproduces the experimental trend of E_a *vs. L* at intermediate L values. For L=1µm we predict DFE_{av}=0.3-0.4 eV (using $6L^2$ or $2L^2$ for the available surface, respectively), which summed to the calculated $\Delta H^{\neq}$ gives E_a values in the 0.4-0.5 eV range, nicely matching the experimental value of ~0.5 eV. [29] In addition, our model predicts the E_a value to saturate to its limit value for large L (~ 1 eV) for grains size larger than ~50 µm. Despite the limits and assumptions, our model works surprisingly well in matching the experimental observables for varying grain sizes and E_a values. Also interesting, the calculated *DFE* for an isolated Frenkel pair in bulk MAPbI$_3$

(1.36 eV, neglecting thermal corrections and entropic contributions) is consistent with the asymptotic value of ~0.9 eV retrieved from analysis of experimental data on single crystals.
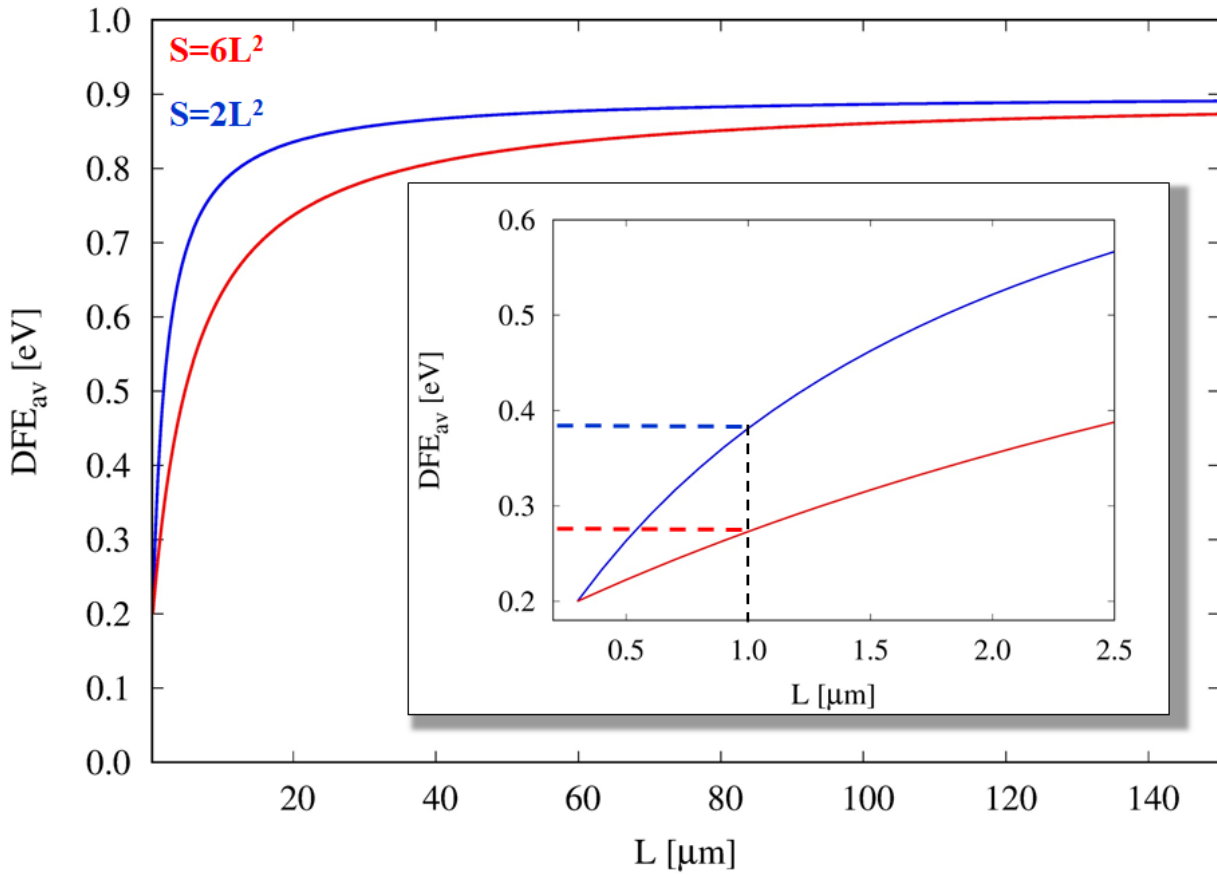
Figure 3. Variation of the defect formation energy (DFE, eV) as a function of crystal grain size (µm) between limiting values of small grains (0.3 µm, bottom left side) and large grains or single crystals (top right side) for two different surface estimates as per Scheme 1 ($6L^2$ and $2L^2$, in red and blue, respectively). The inset shows a zoom in the low L value region, highlighting the results of the model for a grain size of 1 µm, using the two surface estimates of the main Figure.

This analysis accounts for the vastly varying E_a values experimentally reported, whereby *different sample preparation methods would yield films of different grain size with different available surface and grain boundaries and associated different DFE*. This calls for ion migration being dominated by surfaces and grain boundaries, as proposed earlier by Huang and coworkers.[45] Our model also reveals that there exists a lower limit to the E_a value measured in conductivity experiments, which

is set by the $\Delta H^{\neq}$ value when the *DFE* term almost vanishes. In this framework, higher E_a values would simply reflect the different surface-available defect densities characteristic of the system under investigation.

These observations further open up the possibility of speculating on the nature of the light induced increase of ionic migration observed in MAPbI$_3$.[18,29] Since light absorption mainly generates free charges in MAPbI$_3$ at room temperature due to the small exciton binding energy,[46, 47] we first computationally assess whether charge trapping at iodine defects may alter their migration energy barriers. In doing so we necessarily need to resort to high level (and computationally demanding) HSE-SOC structural relaxations, see Supporting Information, since at the PBE (or PBE-SOC) level no trapping occurs at such defects due to misplaced band edges.[11] As reported in Table 1, migration of neutral interstitial iodine (I_i^0) - the species formed upon charge trapping at charged interstitial iodine - is found to be slightly more energetically demanding than migration of I_i^-, 0.18 *vs.* 0.12 eV, respectively. Our calculations also predict V_I^0 migration to have the same barrier than V_I^+ (0.17 eV). Thus upon carrier trapping at iodine defects, *ab initio* calculations predict the migration barriers to either increase or to remain constant, inconsistent with the enhanced ion migration experimentally observed. The overall picture is rather consistent with the formation of defects under light being energetically favored compared to defect formation in the dark, as proposed earlier by Motti *et al.*[48] In addition, our analysis indicates that (light-induced) defect formation prevalently takes place at the surfaces or grain boundaries, calling for proper passivation strategies as a mean to control ion migration and light-induced defect formation in MHPs. Formation of interstitial iodine defects, precursors to I_2 formation and its subsequent loss, was indeed found to be significantly favored at the surface of MAPbI$_3$ compared to the bulk. [11]

In summary, we have provided a model of surface-assisted defect formation which consistently accounts for the spread in experimentally measured activation energies for ion migration in lead-halide perovskites. Key to our model is the introduction of a phenomenological defect formation energy which varies between limiting surface and bulk values as a function of the

surface to volume ratio of crystal grains; and accurate *ab initio* calculations of defect formation energies and migration barriers.

Our findings suggest that surface passivation has a leading role in stabilizing lead-halide perovskites against formation of defects. This may in turn prevent the associated photochemical decomposition reactions, providing the framework for interpreting the bizarre ion conduction properties and light-induced instability of this class of materials. We hope this understanding will further advance the potential of reaching sufficient stability to lead to the launch of commercial products based on MHPs.

Supporting Information Available: Computational details. Migration energy barriers on MAI- and PbI_2-terminated surfaces.

References:

1. Xing, G.; Mathews, N.; Sun, S.; Lim, S. S.; Lam, Y. M.; Grätzel, M.; Mhaisalkar, S.; Sum, T. C. Long-Range Balanced Electron- and Hole-Transport Lengths in Organic-Inorganic CH3NH3PbI3. *Science* **2013,** *342*, 344-347.
2. Stranks, S. D.; Eperon, G. E.; Grancini, G.; Menelaou, C.; Alcocer, M. J. P.; Leijtens, T.; Herz, L. M.; Petrozza, A.; Snaith, H. J. Electron-Hole Diffusion Lengths Exceeding 1 Micrometer in an Organometal Trihalide Perovskite Absorber. *Science* **2013,** *342*, 341-344.
3. Conings, B.; Drijkoningen, J.; Gauquelin, N.; Babayigit, A.; D'Haen, J.; D'Olieslaeger, L.; Ethirajan, A.; Verbeeck, J.; Manca, J.; Mosconi, E. Intrinsic thermal instability of methylammonium lead trihalide perovskite. *Adv. Energy Mater.* **2015,** *5*, 1500477.
4. Yin, W.-J.; Shi, T.; Yan, Y. Unusual defect physics in CH3NH3PbI3 perovskite solar cell absorber. *Appl. Phys. Lett.* **2014,** *104*, 063903.
5. Stranks, S. D.; Burlakov, V. M.; Leijtens, T.; Ball, J. M.; Goriely, A.; Snaith, H. J. Recombination Kinetics in Organic-Inorganic Perovskites: Excitons, Free Charge, and Subgap States. *Phys. Rev. Applied* **2014,** *2*, 034007.
6. Meggiolaro, D.; Motti, S. G.; Mosconi, E.; Barker, A. J.; Ball, J.; Andrea Riccardo Perini, C.; Deschler, F.; Petrozza, A.; De Angelis, F. Iodine chemistry determines the defect tolerance of lead-halide perovskites. *Energy Environ. Sci.* **2018,** *11*, 702-713.
7. Steirer, K. X.; Schulz, P.; Teeter, G.; Stevanovic, V.; Yang, M.; Zhu, K.; Berry, J. J. Defect Tolerance in Methylammonium Lead Triiodide Perovskite. *ACS Energy Lett.* **2016,** *1*, 360-366.

8. Walsh, A.; Zunger, A. Instilling defect tolerance in new compounds. *Nat Mater* **2017,** *16*, 964.

9. Du, M.-H. Density Functional Calculations of Native Defects in CH₃NH₃PbI₃: Effects of Spin–Orbit Coupling and Self-Interaction Error. *J. Phys. Chem. Lett.* **2015,** *6*, 1461-1466.

10. Aristidou, N.; Eames, C.; Sanchez-Molina, I.; Bu, X.; Kosco, J.; Islam, M. S.; Haque, S. A. Fast oxygen diffusion and iodide defects mediate oxygen-induced degradation of perovskite solar cells. *Nat Commun* **2017,** *8*, 15218.

11. Meggiolaro, D.; De Angelis, F. First-Principles Modeling of Defects in Lead Halide Perovskites: Best Practices and Open Issues. *ACS Energy Lett.* **2018,** *3*, 2206-2222.

12. Xiao, Z.; Yuan, Y.; Shao, Y.; Wang, Q.; Dong, Q.; Bi, C.; Sharma, P.; Gruverman, A.; Huang, J. Giant Switchable Photovoltaic Effect in Organometal Trihalide Perovskite Devices. *Nat. Mater.* **2014,** *14*, 193-198.

13. Azpiroz, J. M.; Mosconi, E.; Bisquert, J.; De Angelis, F. Defect migration in methylammonium lead iodide and its role in perovskite solar cell operation. *Energy Environ. Sci.* **2015,** *8*, 2118-2127.

14. Eames, C.; Frost, J. M.; Barnes, P. R. F.; O'Regan, B. C.; Walsh, A.; Islam, M. S. Ionic transport in hybrid lead iodide perovskite solar cells. *Nat Commun* **2015,** *6*, 7497.

15. Mosconi, E.; Meggiolaro, D.; Snaith, H. J.; Stranks, S. D.; De Angelis, F. Light-induced annihilation of Frenkel defects in organo-lead halide perovskites. *Energy Environ. Sci.* **2016,** *9*, 3180-3187.

16. Birkhold, S. T.; Precht, J. T.; Liu, H.; Giridharagopal, R.; Eperon, G. E.; Schmidt-Mende, L.; Li, X.; Ginger, D. S. Interplay of Mobile Ions and Injected Carriers Creates Recombination Centers in Metal Halide Perovskites under Bias. *ACS Energy Lett.* **2018,** *3*, 1279-1286.

17. Meggiolaro, D.; Mosconi, E.; De Angelis, F. Modeling the Interaction of Molecular Iodine with MAPbI3: A Probe of Lead-Halide Perovskites Defect Chemistry. *ACS Energy Lett.* **2018**, 447-451.

18. Kim, G. Y.; Senocrate, A.; Yang, T.-Y.; Gregori, G.; Grätzel, M.; Maier, J. Large tunable photoeffect on ion conduction in halide perovskites and implications for photodecomposition. *Nat Mater* **2018,** *17*, 445-449.

19. Mosconi, E.; De Angelis, F. Mobile Ions in Organohalide Perovskites: Interplay of Electronic Structure and Dynamics. *ACS Energy Lett.* **2016,** *1*, 182-188.

20. Meloni, S.; Moehl, T.; Tress, W.; Franckevicius, M.; Saliba, M.; Lee, Y. H.; Gao, P.; Nazeeruddin, M. K.; Zakeeruddin, S. M.; Rothlisberger, U.; Graetzel, M. Ionic polarization-induced current-voltage hysteresis in CH₃NH₃PbX₃ perovskite solar cells. *Nat Commun* **2016,** *7*, 10334.

21. Luo, Y.; Khoram, P.; Brittman, S.; Zhu, Z.; Lai, B.; Ong, S. P.; Garnett, E. C.; Fenning, D. P. Direct Observation of Halide Migration and its Effect on the Photoluminescence of Methylammonium Lead Bromide Perovskite Single Crystals. *Adv. Mater.* **2017,** *29*, 1703451.

22. Senocrate, A.; Moudrakovski, I.; Kim, G. Y.; Yang, T.-Y.; Gregori, G.; Grätzel, M.; Maier, J. The Nature of Ion Conduction in Methylammonium Lead Iodide: A Multimethod Approach. *Angew. Chemie Int. Ed.* **2017,** *56*, 7755-7759.

23. Li, C.; Tscheuschner, S.; Paulus, F.; Hopkinson, P. E.; Kießling, J.; Köhler, A.; Vaynzof, Y.; Huettner, S. Iodine Migration and its Effect on Hysteresis in Perovskite Solar Cells. *Adv. Mater.* **2016,** *28*, 2446-2454.

24. Yuan, Y.; Chae, J.; Shao, Y.; Wang, Q.; Xiao, Z.; Centrone, A.; Huang, J. Photovoltaic Switching Mechanism in Lateral Structure Hybrid Perovskite Solar Cells. *Adv. Energy Mater.* **2015,** *5*, 1500615.

25. Haruyama, J.; Sodeyama, K.; Han, L.; Tateyama, Y. First-Principles Study of Ion Diffusion in Perovskite Solar Cell Sensitizers. *J. Am. Chem. Soc.* **2015,** *137*, 10048-10051.

26. Yang, J.-H.; Yin, W.-J.; Park, J.-S.; Wei, S.-H. Fast self-diffusion of ions in CH3NH3PbI3: the intersticaly mechanism versus vacancy-assisted mechanism. *J. Mater. Chem. A* **2016,** *4*, 13105-13112.

27. Pazoki, M.; Wolf, M. J.; Edvinsson, T.; Kullgren, J. Vacancy dipole interactions and the correlation with monovalent cation dependent ion movement in lead halide perovskite solar cell materials. *Nano Energy* **2017,** *38*, 537-543.

28. Oranskaia, A.; Yin, J.; Bakr, O. M.; Brédas, J.-L.; Mohammed, O. F. Halogen Migration in Hybrid Perovskites: The Organic Cation Matters. *J. Phys. Chem. Lett.* **2018,** *9*, 5474-5480.

29. Xing, J.; Wang, Q.; Dong, Q.; Yuan, Y.; Fang, Y.; Huang, J. Ultrafast ion migration in hybrid perovskite polycrystalline thin films under light and suppression in single crystals. *Phys. Chem. Chem. Phys.* **2016,** *18*, 30484-30490.

30. Hoke, E. T.; Slotcavage, D. J.; Dohner, E. R.; Bowring, A. R.; Karunadasa, H. I.; McGehee, M. D. Reversible Photo-Induced Trap Formation in Mixed-Halide Hybrid Perovskites for Photovoltaics. *Chem. Sci.* **2014,** *6*, 613-617.

31. Barker, A. J.; Sadhanala, A.; Deschler, F.; Gandini, M.; Senanayak, S. P.; Pearce, P. M.; Mosconi, E.; Pearson, A. J.; Wu, Y.; Srimath Kandada, A. R.; Leijtens, T.; De Angelis, F.; Dutton, S. E.; Petrozza, A.; Friend, R. H. Defect-Assisted Photoinduced Halide Segregation in Mixed-Halide Perovskite Thin Films. *ACS Energy Lett.* **2017,** *2*, 1416-1424.

32. Yoon, S. J.; Kuno, M.; Kamat, P. V. Shift Happens. How Halide Ion Defects Influence Photoinduced Segregation in Mixed Halide Perovskites. *ACS Energy Lett.* **2017,** *2*, 1507-1514.

33. C., M.; D., G.; R., S. PRE-EXPONENTIAL TERM IN THE ARRHENIUS EQUATION FOR ELECTRICAL CONDUCTIVITY OF GLASS. *Journal de Physique Colloques* **1982,** *43*, C9-395-C9-398.

34. Murali, B.; Yengel, E.; Yang, C.; Peng, W.; Alarousu, E.; Bakr, O. M.; Mohammed, O. F. The Surface of Hybrid Perovskite Crystals: A Boon or Bane. *ACS Energy Lett.* **2017,** *2*, 846-856.

35. Murali, B.; Dey, S.; Abdelhady, A. L.; Peng, W.; Alarousu, E.; Kirmani, A. R.; Cho, N.; Sarmah, S. P.; Parida, M. R.; Saidaminov, M. I.; Zhumekenov, A. A.; Sun, J.; Alias, M. S.; Yengel, E.; Ooi, B. S.; Amassian, A.; Bakr, O. M.; Mohammed, O. F. Surface Restructuring of Hybrid Perovskite Crystals. *ACS Energy Lett.* **2016,** *1*, 1119-1126.

36. Birkhold, S. T.; Precht, J. T.; Giridharagopal, R.; Eperon, G. E.; Schmidt-Mende, L.; Ginger, D. S. Direct Observation and Quantitative Analysis of Mobile Frenkel Defects in Metal Halide Perovskites Using Scanning Kelvin Probe Microscopy. *J. Phys. Chem. C* **2018,** *122*, 12633-12639.

37. Chen, B.; Li, T.; Dong, Q.; Mosconi, E.; Song, J.; Chen, Z.; Deng, Y.; Liu, Y.; Ducharme, S.; Gruverman, A.; Angelis, F. D.; Huang, J. Large electrostrictive response in lead halide perovskites. *Nat Mater* **2018,** *17*, 1020–1026.

38. Uratani, H.; Yamashita, K. Charge Carrier Trapping at Surface Defects of Perovskite Solar Cell Absorbers: A First-Principles Study. *J. Phys. Chem. Lett.* **2017,** *8*, 742-746.

39. Grimme, S.; Antony, J.; Ehrlich, S.; Krieg, H. A consistent and accurate ab initio parametrization of density functional dispersion correction (DFT-D) for the 94 elements H-Pu. *J. Chem. Phys.* **2010,** *132*, 154104.

40. Kim, M.; Motti, S. G.; Sorrentino, R.; Petrozza, A. Enhanced solar cell stability by hygroscopic polymer passivation of metal halide perovskite thin film. *Energy Environ. Sci.* **2018,** *11*, 2609-2619.

41. Belisle, R. A.; Bush, K. A.; Bertoluzzi, L.; Gold-Parker, A.; Toney, M. F.; McGehee, M. D. Impact of Surfaces on Photoinduced Halide Segregation in Mixed-Halide Perovskites. *ACS Energy Lett.* **2018,** 2694-2700.

42. deQuilettes, D. W.; Vorpahl, S. M.; Stranks, S. D.; Nagaoka, H.; Eperon, G. E.; Ziffer, M. E.; Snaith, H. J.; Ginger, D. S. Impact of microstructure on local carrier lifetime in perovskite solar cells. *Science* **2015,** *348*, 683-686.

43. Noel, N. K.; Abate, A.; Stranks, S. D.; Parrott, E. S.; Burlakov, V. M.; Goriely, A.; Snaith, H. J. Enhanced Photoluminescence and Solar Cell Performance via Lewis Base Passivation of Organic–Inorganic Lead Halide Perovskites. *ACS Nano* **2014,** *8*, 9815-9821.

44. Abate, A.; Saliba, M.; Hollman, D. J.; Stranks, S. D.; Wojciechowski, K.; Avolio, R.; Grancini, G.; Petrozza, A.; Snaith, H. J. Supramolecular Halogen Bond Passivation of Organic–Inorganic Halide Perovskite Solar Cells. *Nano Lett.* **2014,** *14*, 3247-3254.

45. Shao, Y.; Fang, Y.; Li, T.; Wang, Q.; Dong, Q.; Deng, Y.; Yuan, Y.; Wei, H.; Wang, M.; Gruverman, A.; Shield, J.; Huang, J. Grain boundary dominated ion migration in polycrystalline organic–inorganic halide perovskite films. *Energy Environ. Sci.* **2016,** *9*, 1752-1759.

46. Mahboubi Soufiani, A.; Yang, Z.; Young, T.; Miyata, A.; Surrente, A.; Pascoe, A.; Galkowski, K.; Abdi-Jalebi, M.; Brenes, R.; Urban, J.; Zhang, N.; Bulovic, V.; Portugall, O.; Cheng, Y.-B.; Nicholas, R. J.; Ho-Baillie, A.; Green, M. A.; Plochocka, P.; Stranks, S. D. Impact of microstructure on the electron-hole interaction in lead halide perovskites. *Energy Environ. Sci.* **2017,** *10*, 1358-1366.

47. Umari, P.; Mosconi, E.; De Angelis, F. Infrared Dielectric Screening Determines the Low Exciton Binding Energy of Metal-Halide Perovskites. *J. Phys. Chem. Lett.* **2018,** *9*, 620-627.

48. Motti, S. G.; Gandini, M.; Barker, A. J.; Ball, J. M.; Srimath Kandada, A. R.; Petrozza, A. Photoinduced Emissive Trap States in Lead Halide Perovskite Semiconductors. *ACS Energy Lett.* **2016,** *1*, 726-730.